Physics and Imaging in Radiation Oncology 31 (2024) 100626

Contents lists available at ScienceDirect

Physics and Imaging in Radiation Oncology

journal homepage: www.sciencedirect.com/journal/physics-and-imaging-in-radiation-oncology

Original Research Article

Delta radiomics to track radiation response in lung tumors receiving stereotactic magnetic resonance-guided radiotherapy

Yining Zha [a,b,c], Zezhong Ye [a,b], Anna Zapaishchykova [a,b,d], John He [b], Shu-Hui Hsu [b], Jonathan E. Leeman [b], Kelly J. Fitzgerald [b], David E. Kozono [b], Raymond H. Mak [a,b], Hugo J.W.L. Aerts [a,b,d,e], Benjamin H. Kann [a,b,*]

[a] Artificial Intelligence in Medicine Program, Mass General Brigham, Harvard Medical School, Boston, MA, USA
[b] Department of Radiation Oncology, Dana-Farber Cancer Institute and Brigham and Women's Hospital, Harvard Medical School, Boston, MA, USA
[c] Department of Biostatistics, Harvard T.H. Chan School of Public Health, Boston, MA, USA
[d] Radiology and Nuclear Medicine, CARIM & GROW, Maastricht University, Maastricht, the Netherlands
[e] Department of Radiology, Brigham and Women's Hospital, Dana-Farber Cancer Institute, Harvard Medical School, Boston, MA, USA

ARTICLE INFO

Keywords:
Delta-radiomics
Lung cancer
Dose response
Survival analysis
SBRT
MRI-guided radiotherapy

ABSTRACT

Background and purpose: Lung cancer is a leading cause of cancer-related mortality, and stereotactic body radiotherapy (SBRT) has become a standard treatment for early-stage lung cancer. However, the heterogeneous response to radiation at the tumor level poses challenges. Currently, standardized dosage regimens lack adaptation based on individual patient or tumor characteristics. Thus, we explore the potential of delta radiomics from on-treatment magnetic resonance (MR) imaging to track radiation dose response, inform personalized radiotherapy dosing, and predict outcomes.

Materials and methods: A retrospective study of 47 MR-guided lung SBRT treatments for 39 patients was conducted. Radiomic features were extracted using Pyradiomics, and stability was evaluated temporally and spatially. Delta radiomics were correlated with radiation dose delivery and assessed for associations with tumor control and survival with Cox regressions.

Results: Among 107 features, 49 demonstrated temporal stability, and 57 showed spatial stability. Fifteen stable and non-collinear features were analyzed. Median Skewness and surface to volume ratio decreased with radiation dose fraction delivery, while coarseness and 90th percentile values increased. Skewness had the largest relative median absolute changes (22 %–45 %) per fraction from baseline and was associated with locoregional failure ($p = 0.012$) by analysis of covariance. Skewness, Elongation, and Flatness were significantly associated with local recurrence-free survival, while tumor diameter and volume were not.

Conclusions: Our study establishes the feasibility and stability of delta radiomics analysis for MR-guided lung SBRT. Findings suggest that MR delta radiomics can capture short-term radiographic manifestations of the intratumoral radiation effect.

1. Introduction

Lung cancer is the leading cause of cancer-related mortality with a 3-year relative survival rate of 33 % in the United States from 2016 to 2018 [1]. Stereotactic body radiotherapy (SBRT) has emerged as a standard treatment modality for early-stage lung cancer in the inoperable setting with high rates of initial local control despite increasing recurrence risk over time [2]. Previous studies demonstrate that pathologic complete response post-SBRT is heterogeneous and lower than anticipated [3], suggesting there may be differential radiation dose responses at the tumor level, even at ablative dose ranges.

Current protocols standardize dosages without accounting for patient or tumor specifics, aiming for a biologically equivalent dose (BED) >= 100 Gy(alpha/beta: 10), with tailored tradeoffs in situations where tumors closely abut critical normal structures [4]. There is currently no direct way to assess radiation dose response during SBRT in vivo, and

* Corresponding authors at: Department of Radiation Oncology, Dana-Farber Cancer Institute and Brigham and Women's Hospital, Harvard Medical School, 75 Francis Street, Boston, MA 02115, USA.
E-mail address: Benjamin_Kann@dfci.harvard.edu (B.H. Kann).

https://doi.org/10.1016/j.phro.2024.100626
Received 22 March 2024; Received in revised form 1 August 2024; Accepted 6 August 2024
Available online 12 August 2024

resultingly little basis for tailoring dose. Improving the ability to track and predict individual, patient-level responses to SBRT would be valuable to inform personalized radiotherapy (RT) dosing regimens, risk-stratification, and selection of patients for adjuvant or neoadjuvant therapy intensification.

RT inflicts damage through DNA double-stranded breaks leading to cell death mechanisms such as apoptosis and necroptosis or tumor necrosis [5]. These cellular changes can manifest hours to days post-RT [5], and it may be possible to indirectly assess these changes via radiographic changes, providing insights into RT dose response [6,7]. Radiomics analyses, which extract quantitative features from imaging data have shown promise for predicting RT response and decision support [8], with the predominant literature assessing baseline radiomic features from pre- and post-treatment imaging to make predictions [9]. *Delta radiomics* model variations in quantitative tumor imaging features *intra-treatment* and can enhance the understanding of radiation dose response and recurrence risk by using sequential images as internal controls for radiographic changes [10]. However, until recently, intra-fractional radiomic analyses were hindered by the low quality of imaging systems like traditional cone beam computer tomography (CT), which suffer from poor soft tissue contrast and signal-to-noise ratios [11].

Recently, magnetic resonance (MR)-guided RT has gained traction for various malignancies, representing an advance for image-guided RT with standardized, real-time fractional MR images with superior soft tissue contrast and tumor visualization and localization than current CT-guided RT. Furthermore, MR-guidance with breath-hold has also been shown to improve image quality [12]. MR-guided RT for lung SBRT, given its standardized dosing regimens and on-treatment imaging protocols, enables systematic investigation of intra-fractional radiographic changes that could potentially lead to reproducible, longitudinal imaging biomarkers of radiation dose response.

Previous research on pancreatic cancer investigated MR delta radiomics and discovered that change in histogram skewness, which represents the asymmetry of voxel intensities about mean intensity, correlated with progression free survival (PFS) [13]. To our knowledge, no published studies have yet explored MR delta radiomics in lung cancer, nor have intra-fractional changes been investigated for dose response with granular endpoints. We sought to address this knowledge gap by investigating a database of patients receiving MR-guided lung SBRT. The aim of this study was to determine the feasibility and stability of MR radiomic feature extraction for lung SBRT. Furthermore, we aimed to investigate how MR delta radiomics is associated with increasing radiation dose delivery and to assess the association between on-treatment changes and tumor control as well as patient survival.

2. Materials and methods

2.1. Dataset and patient population

We conducted a retrospective study of patients treated with MR-guided lung SBRT at our institution since the inception of our MR-guided RT program in 2019 with database abstraction in October 2022 (Fig. 1). All patients were treated with five RT fractions, delivered every other weekday, per institutional protocol. This study was conducted under the Declaration of Helsinki guidelines and was approved by the institutional internal review board (IRB) with a waiver of consent. Treatment was administered using the ViewRay MRIdian 0.35T system for Stereotactic MR-guided adaptive radiation therapy (SMART), as per previously described methods [12]. Inclusion criteria were treatment for lung tumors (primary or metastasis) with complete imaging records, including an MR simulation and 5 pre-treatment scans from fractions one through five. Clinical outcomes such as survival status, radiation start date, locoregional control, and distant metastasis status were abstracted by a trained clinical research coordinator in a Research Electronic Data Capture database and verified by a board-certified radiation oncologist (B.H.K.). For patients with multiple primaries treated, analysis was conducted by treatment course. Reporting follows the Transparent Reporting of a Multivariable Prediction Model for Individual Prognosis (TRIPOD) guidelines [14].

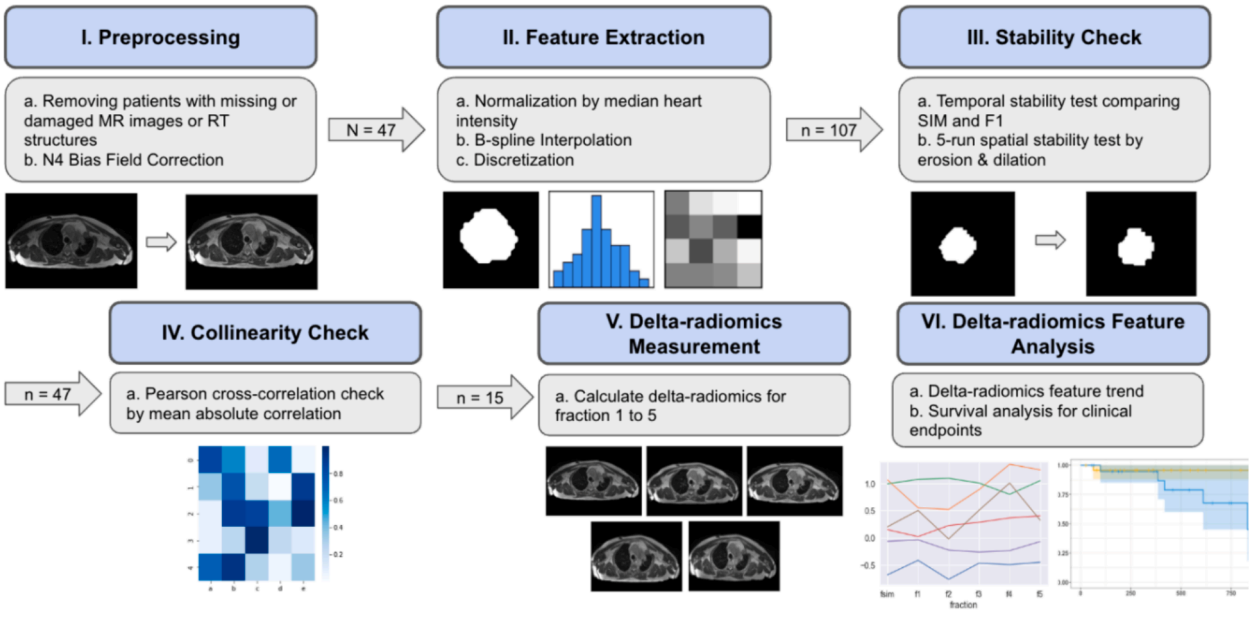

Fig. 1. Study framework. N indicates number of patients in the study. N indicates number of features after each step. I. Preprocessing. Images before (left) and after (right) show the change after N4 bias field correction. II. Feature Extraction. Three types of features were extracted after preprocessing: shape-based features (left), first-order histogram features (middle), and texture features (right). III. Stability Check. Images before (left) and after (right) show the shape change of tumor after erosion and dilation. IV. Collinearity check. Heatmap for feature Pearson correlation. V. Delta-radiomics Measurement. Delta-radiomics were calculated for fractions 1 (top left), 2 (top middle), 3 (top right), 4 (bottom left), 5 (bottom right). For analysis of radiation dose–response, delta-radiomics were calculated using the formula (Fn – F1)/F1, where Fn represents the fraction number. For analysis of disease outcome, delta-radiomic slope (F5/F1) was used. VI. Delta-radiomics Feature Analysis. Relative trend of feature among fractions (left) and Kaplan-Meier for survival analysis (right).

2.2. Patient characteristics

In this study, 47 MR-guided lung SBRT treatments for 39 patients were analyzed (Table 1), with 22 (47 %) in the setting of Stage IV disease. With a median follow-up time of 415 days (range: 32–1178 days), 17 deaths (36 %), 25 progression events (53 %), 6 locoregional failure events (13 %), and specifically 4 in-field locoregional failure events (9 %) were observed. Each of the six patients with locoregional failures underwent one treatment course. Radiation total dose delivered ranged from 40 Gy to 60 Gy in 5 fractions (dose per fraction range: 8 Gy/fx to 12 Gy/fx). One patient had reirradiation to an overlapping area (24 months after prior course). Eight patients received systemic chemotherapy after SBRT.

2.3. Image acquisition

MR images were acquired in DICOM format on the ViewRay MRIdian system at pretreatment simulation (F0) and before each subsequent RT fraction (F1-5) with true fast imaging with steady-state precession (TrueFISP) sequence using 144 slices, and voxel size $1.5 \times 1.5 \times 3$ mm, with repetition time (TR) = 3 ms and echo time (TE) = 1.27 ms. Images were acquired in an inspiration breath-hold position. Gross tumor volume (GTV) regions of interest (ROIs) were contoured at simulation and aligned to the daily MR scans, and if needed, modified, and confirmed daily by treating radiation oncologists at the time of planning via the MR images.

2.4. Radiomics pipeline

Radiomic feature extraction was performed by the Pyradiomics package [15] in Python 3.9.1 per Image Biomarker Standardisation Initiative (IBSI) guidelines [16]. All DICOM images and structures were converted to NIFTI with N4 bias field correction applied before extraction via SimpleITK [17] in Python. Intensity values were quantized with bin count 64 and B-spline interpolation was used to resample images. Normalization in the Pyradiomics pipeline was modified by dividing the intensity of each image by the corresponding median heart intensity value acquired from each thoracic MR. This method controls global intensity variation among fractions [13]. Median lung intensity value was not considered for normalization because tumors in lung could alter signal intensity. Median heart intensities were extracted for all fractions per patient. A total of 107 radiomic features for every scan were extracted from 7 classes (Table S1).

2.5. Radiomics stability

Radiomic feature stability was evaluated both temporally and spatially. Temporal stability was evaluated by comparing feature values acquired at simulation (SIM) and F1 within two weeks without radiation. Spatial stability was evaluated via random erosions and dilations of the GTV contour to simulate small, expected discrepancies between clinicians. Random contouring perturbations were repeated five times to avoid potential bias (Table S1). Stability was assessed via Lin's Concordance Correlation Coefficient (CCC), with a value > 0.90 indicating stability.

Collinearity was assessed using Pearson correlation, identifying pairs with correlation >0.90.

In each pair, the feature with a higher mean absolute correlation across all other features was dropped to mitigate collinearity effects. The remaining stable, non-collinear features underwent delta radiomics analysis, evaluating relative changes between RT fractions, normalized by the initial fraction's value (e.g., (F2-F1)/F1). This process also included calculating delta ratios from start to finish (F5/F1) and identifying features with consistent changes as potential indicators of RT-induced cellular change. Additionally, an analogous analysis of absolute changes in feature values was performed (Supplemental Methods 2,

Table 1
Patient and tumor characteristics.

Patient and Treatment Characteristics		N = 47 treatments (39 patients)
Age at time of treatment, median (IQR)		67 (61.5–73.5)
Sex		
	Female	27 (57 %)
	Male	20 (43 %)
Smoking status		
	Former smoker (quit >1 year prior to diagnosis)	33 (70 %)
	Never smoker (<100 cigarettes in lifetime)	10 (21 %)
	Current smoker (smoking at time of diagnosis or quit <1 year prior)	3 (6 %)
	Unspecified	1 (2 %)
Performance status		
	0	23 (49 %)
	1	21 (45 %)
	2	2 (4 %)
	Unspecified	1 (2 %)
Prior thoracic RT		
	Yes	19 (40 %)
	No	22 (47 %)
	Unspecified	6 (13 %)
T stage		
	T0	0 (0 %)
	T1a	12 (26 %)
	T1b	5 (11 %)
	T2a	1 (2 %)
	T2b	2 (4 %)
	T3	6 (13 %)
	T4	3 (6 %)
	Unspecified	18 (38 %)
N stage		
	N0	27 (57 %)
	N1	1 (2 %)
	N2	0 (0 %)
	N3	1 (2 %)
	Unspecified	18 (38 %)
M stage		
	M0	25 (53 %)
	M1	22 (47 %)
Overall stage		
	I	15 (32 %)
	II	7 (15 %)
	III	3 (6 %)
	IV	22 (47 %)
Recurred tumor		
	No	37 (79 %)
	Yes, reirradiation	1 (2 %)
	Yes, not reirradiation	9 (19 %)
Tumor size as radiographically measured at diagnosis, cm (median, IQR)		1.6 (1.3–2.5)
Maximum 3D tumor diameter extracted from GTV, cm (median, IQR)		3.7 (3.0–5.0)

(*continued on next page*)

Table 1 (*continued*)

Patient and Treatment Characteristics		N = 47 treatments (39 patients)
Tumor volume, cm^3 (median, IQR)		8.6 (4.3–15.1)
Histology		
	Metastasis from other site	15 (32 %)
	Adenocarcinoma	14 (30 %)
	No pathology	12 (26 %)
	Mesothelioma	3 (6 %)
	Large cell carcinoma	2 (4 %)
	Other	1 (2 %)
Radiation total dose delivered (Gy)		
	40	4 (9 %)
	50	28 (60 %)
	55	3 (6 %)
	60	12 (26 %)
Radiation dose per fraction (Gy/fx)		
	8	4 (9 %)
	10	28 (60 %)
	11	3 (6 %)
	12	12 (26)
Biologically equivalent dose to tumor (Gy10)		
	72	4 (9 %)
	100	26 (55 %)
	115.5	3 (6 %)
	132	13 (28 %)
	300	1 (2 %)
Reirradiation		
	Yes	1 (2 %)
	No	46 (98 %)
Concurrent chemotherapy		
	Yes	0 (0 %)
	No	39 (83 %)
	Unspecified	8 (17 %)
Adjuvant chemotherapy		
	Yes	8 (17 %)
	No	31 (66 %)
	Unspecified	8 (17 %)

Multiple treatments of one patient are considered independent cases. Median of age excluded unspecified patients. IQR: interquartile range, GTV: gross tumor volume. Maximum 3D diameter was extracted via Pyradiomics package using the 3D Feret Diameter. Metastasis from other site included sarcoma, colorectal cancer, melanoma, esophageal cancer, head and neck cancer, and other cancer.

Fig. S6, Table S10–S12).

2.6. Clinical endpoints

Association of delta radiomic slope (F5/F1) for the final stable and non-collinear features and disease outcomes were evaluated for overall survival (OS), progression-free survival (PFS), local-failure free survival (LFFS), and in-field LFFS (iLFFS). iLFFS is defined as >20 % increase in longest diameter compared to nadir of disease extent after treatment and/or biopsy-proven and/or residual (equal to or greater than pre-treatment) or new Fludeoxyglucose F18 (FDG) uptake on positron emission tomography (PET). Event timing was from radiation start to occurrence. Follow-ups followed National Comprehensive Cancer Network (NCCN) guidelines, with CT surveillance generally every 3 months and assessments by Response Evaluation Criteria in Solid Tumors (RECIST).

2.7. Statistical analysis

Delta radiomic trends were analyzed by median relative change between fractions. The analysis of covariance (ANCOVA) compared patients based on locoregional failure for relative F5/F1 skewness by base R package in R V.4.3.1. Univariate and multivariate survival analyses were performed for clinical endpoints via the Lifelines package V.0.27.7 in Python. Univariate Cox proportional hazard regression model evaluated the effect of each delta radiomics ratio (F5/F1) on outcomes. Benjamini-Hochberg correction [18] applied for multiple testing corrections. Feature selection with Recursive Feature Elimination (RFE) [19] with Lasso Regression was applied for feature selection to control the number of features and avoid overfitting the multivariate Cox model. The final Cox model incorporated covariates from the top four feature rankings to reflect the feature importance [20]. Given the prior observation of change in Skewness as a PFS predictor for pancreatic cancer [13], we attempted to validate this feature in our lung cancer cohort. This involved assessing Skewness against disease outcomes at the established cutoff of F5/F1 = 0.951 [13] and through a conditional inference tree for LFFS within our cohort using the partykit package in R. Disease outcomes were compared using Kaplan-Meier plots and log-rank tests, considering $p < 0.05$ as statistically significant.

3. Results

3.1. MR delta radiomics and radiation dose–response

From 107 features extracted, 49 (46 %) demonstrated temporal stability, 57 (53 %) demonstrated spatial stability, and 47 (44 %) demonstrated both (Table S1). Among these, 15 non-collinear features were identified (Fig. S1). Stable and non-collinear delta radiomic features demonstrated heterogeneous intra-fraction trajectories across patients (Fig. 2). Most features exhibited a mix of increasing and decreasing feature values per fraction (Fig. 2). Notably, Skewness and SurfaceVolumeRatio most often decreased from F1 to F5 (64 %, and 55 % of tumors, respectively) across tumors (Fig. 2, Table S2). In contrast, Coarseness and 90 Percentile were the most likely to increase with radiation dose (62 % and 60 % of cases, respectively, Table S2). To illustrate the variability in Skewness change, GIFs were provided to show the patient with the largest Skewness change from F1 to F5 and the patient with the smallest Skewness change from F1 to F5 (Fig. S2). 3D tumor volume (VoxelVolume), while excluded from the final 15 features due to collinearity, was analyzed separately due to its clinical importance and associations with long-term RT response [21] (Supplemental Methods 1, Fig. S3, Table S6–S9). For all delta radiomic features, across patients, there were substantial portions of patients with all positive (median: +21 %, range: +9% to +36 %) or all-negative (median: −21 %, range: −9% to −30 %) relative radiomic value changes for F2 through F5 compared to the F1 baseline (Fig. S4, Table S3). Textural feature, GrayLevelNonUniformity, for which lower values indicate more homogeneity [15] demonstrated consistent negative median change per fraction, and one feature, LargeDependenceHighGrayLevelEmphasis, which indicates concentration of high-intensity voxel values, showed a consistent median increase per fraction (Table S4). Skewness, along with these two features, had the largest median absolute changes per fraction on-treatment (Table 2) and the largest magnitude of median relative dose-related change from baseline (22 % to 45 %) (Table 2). Analysis of radiomic feature absolute value changes demonstrated similar results (Supplemental Methods 2, Fig. S6, Table S10–S12).

3.2. Delta radiomics and disease outcome

For the stable and non-collinear features, univariable survival analysis of four clinical endpoints using feature delta radiomic slope (F5/F1) was examined (Table S5). Initially, we observed significant associations of delta Elongation ($p = 0.006$), Flatness ($p = 0.03$), and Skewness (p =

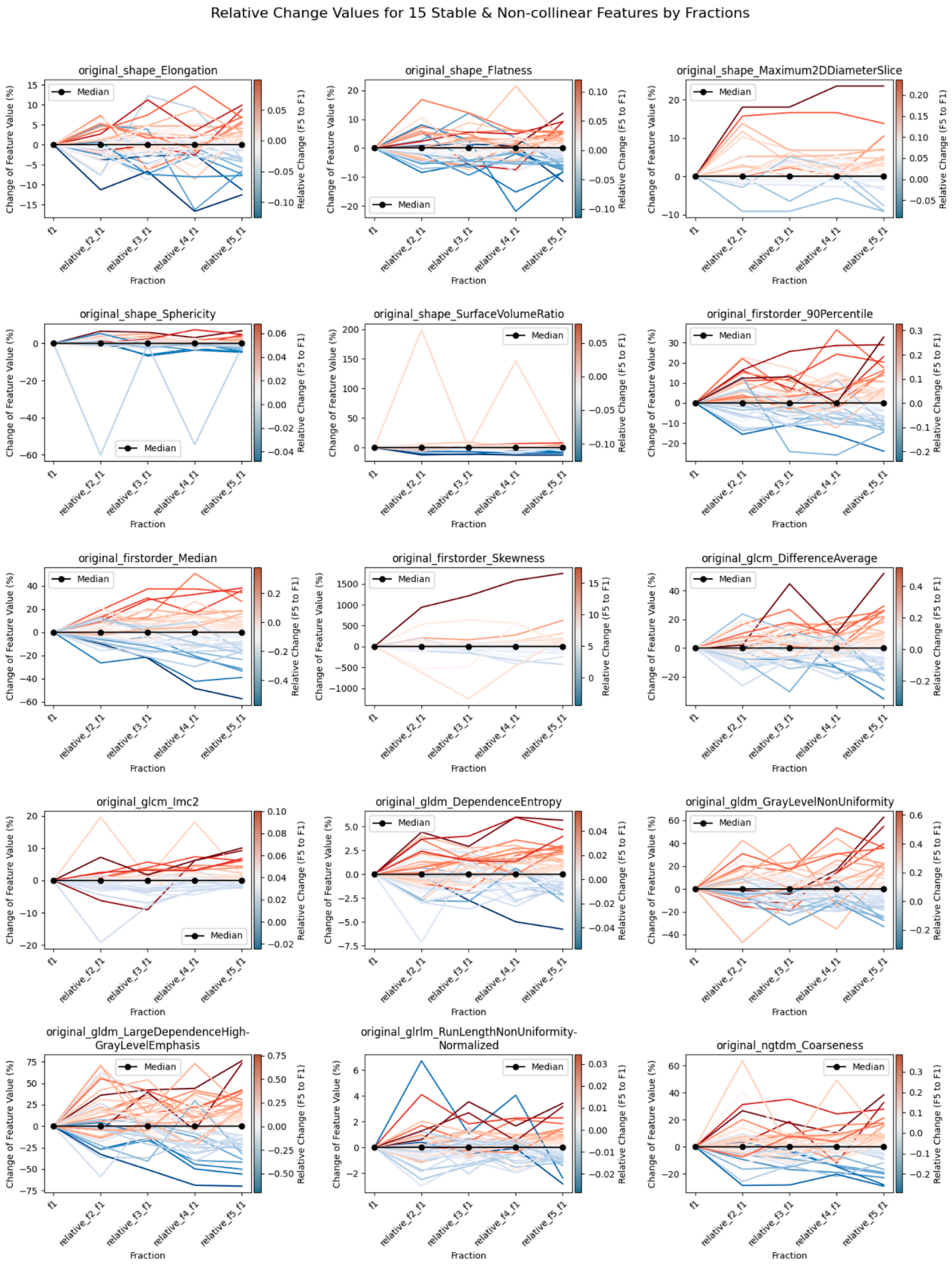

Fig. 2. Delta radiomics trends for stable, non-collinear features across all treatment courses (n = 47), showing relative feature changes of feature values across fractions. The dotted black line shows median values of relative value for each fraction. Gradient color legend and color of lines show the value of relative F5 over F1 for each feature.

Table 2
Relative median and IQR of absolute change for 15 stable and non-collinear features across fractions 1 to 5 (normalized by fraction 1).

Feature Name	F2 (%)	F3 (%)	F4 (%)	F5 (%)
Skewness	21.79 (10.42, 85.24)	41.33 (20.49, 72.96)	40.38 (20.45, 118.55)	45.41 (22.41, 94.31)
LargeDependenceHighGrayLevelEmphasis	16.71 (4.47, 26.98)	12.50 (5.66, 24.54)	20.95 (9.12, 31.33)	18.95 (10.63, 29.83)
GrayLevelNonUniformity	8.07 (4.57, 13.24)	8.76 (5.38, 15.43)	9.79 (4.53, 15.58)	11.41 (4.94, 21.54)
DifferenceAverage	7.94 (3.42, 11.15)	6.01 (3.51, 9.35)	5.62 (2.91, 10.14)	8.76 (3.59, 18.45)
Median	8.10 (3.85, 12.45	8.09 (3.15, 13.66)	9.56 (4.26, 16.59)	7.71 (2.95, 17.23)
90Percentile	5.67 (2.08, 10.45)	5.13 (2.61, 11.00)	5.06 (2.38, 10.98)	7.15 (3.62, 13.42)
Coarseness	5.20 (2.51, 9.53)	5.78 (2.49, 9.76)	6.56 (3.52, 10.91)	5.95 (2.72, 15.99)
Flatness	2.00 (0.42, 4.94)	2.70 (1.11, 5.43)	2.00 (0.75, 4.75)	2.79 (1.38, 5.69)
Elongation	1.58 (0.66, 3.60)	2.33 (0.59, 4.79)	1.83 (0.48, 3.39)	2.10 (0.59, 4.75)
Maximum2DDiameterSlice	0.00 (0.00, 2.59)	1.18 (0.00, 4.62)	0.00 (0.00, 2.67)	1.09 (0.00, 3.96)
Imc2	0.93 (0.33, 2.11)	1.04 (0.23, 2.80)	0.92 (0.35, 3.04)	1.05 (0.30, 1.91)
DependenceEntropy	1.28 (0.46, 2.53)	1.37 (0.80, 1.84)	1.38 (0.48, 2.43)	1.04 (0.67, 2.26)
Sphericity	0.61 (0.17, 1.67)	0.84 (0.33, 2.03)	0.60 (0.21, 1.62)	0.95 (0.41, 2.46)
SurfaceVolumeRatio	1.05 (0.24, 3.09)	1.13 (0.50, 2.38)	0.66 (0.20, 2.30)	0.79 (0.33, 1.99)
RunLengthNonUniformityNormalized	0.72 (0.32, 1.18)	0.57 (0.36, 1.12)	0.53 (0.25, 0.95)	0.75 (0.39, 1.16)

Median values were calculated by relative feature absolute values. Features were ordered by relative F5 over F1 values, showing intra-fraction fluctuations.

0.01) with locoregional failure free survival (LFFS); Imc2 ($p = 0.04$) for progression free survival (PFS), and GrayLevelNonUniformity with overall survival (OS) ($p = 0.049$). However, no significant associations remained after correction for multiple hypotheses. Ratio of Skewness, previously observed as statistically significant for PFS in pancreatic cancer (Tomaszewski et al., 2021), trended towards LFFS correlation ($p = 0.01$, corrected $p = 0.09$) in our study, indicating higher Skewness slopes might associate with worse outcomes. Additionally, ANCOVA confirmed Skewness's association with locoregional failure (p = 0.01). The relative changes of feature Skewness from F1 to F5 for cases with (n = 6) and without (n = 41) locoregional failure highlighted the sensitivity of its relative value to dose change in both groups (Fig. S5). Tumor volume had no observed association with disease outcomes (Table S9).

We further investigated the optimal threshold for relative skewness change as a marker for local control. A conditional inference tree using recursive partitioning demonstrated maximal separation to divide patients into low-risk (n = 28) and high-risk (n = 19) groups of LFFS at an optimal threshold of skewness ratio = 0.973 (Fig. 3). Survival plots showed a numerical but not statistically significant differentiation between these groups at these thresholds (Fig. 3).

For multivariable Cox regression with RFE, we found that F5/F1 ratio of feature Elongation, which shows the relationship between the two largest principal components in the GTV shape, was selected to fit the model in all 4 clinical endpoints. Covariates F5/F1 ratio of Elongation and original_glcm_Imc2 were all significantly associated with PFS (HR 1.21 [95 % CI 1.01–1.45], $p = 0.04$; HR 1.2 [95 % CI 1.04–1.39], p

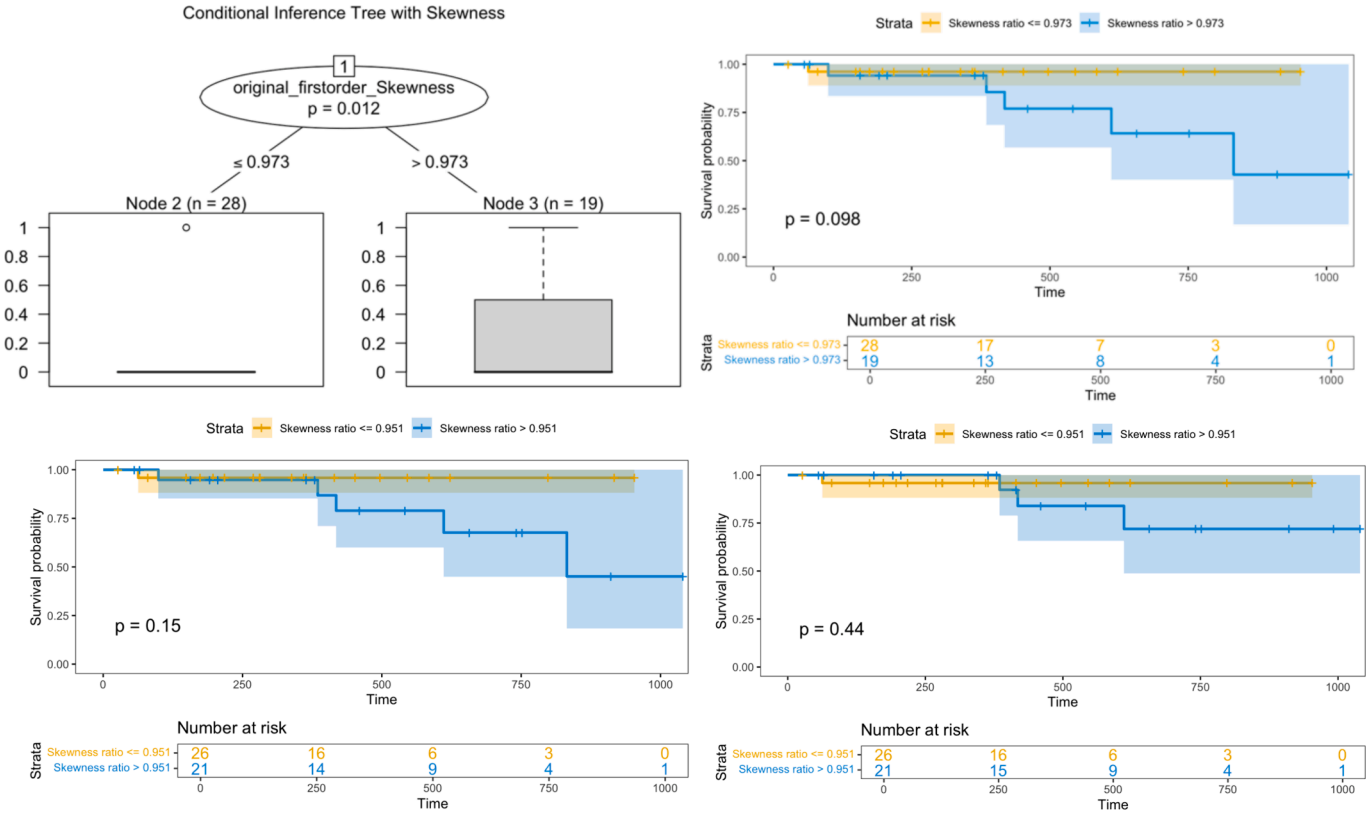

Fig. 3. Conditional inference tree and Kaplan-Meier plot for feature skewness between F5 and F1. Upper Left: Conditional inference tree for LFFS with optimal cutoff point skewness = 0.973. Upper right: Measure the optimal cutoff point for LFFS. Bottom left: Test cutoff point skewness = 0.951 for LFFS. Bottom right: Test cutoff point skewness = 0.951 for ILFFS.

= 0.01)) and covariates F5/F1 ratio of Elongation was also significantly associated with LFFS (HR=1.7 [95 % CI 1.10–2.65], p = 0.02) (See Table 3).

4. Discussion

Radiation-induced tumor intra- and extra-cellular response may manifest radiographically, and the ability to practically measure and evaluate these changes would significantly advance personalized treatment. MR-guided RT, known for its high-quality intra-fraction imaging and standardized procedures, alongside advanced radiomics approaches, holds promise for detecting and tracking radiation dose effect. To our knowledge, this study marks the first systematic exploration of MR radiomic intra-treatment changes for lung tumors, adding to the emerging field of MR-guided RT delta-radiomics. In this proof-of-principle study, we found that delta radiomic feature extraction can be feasible, stable, and reproducible on a low-field, 0.35 T MRI-guided linear accelerator. Analyzing 15 such features, we observed varied and distinct patient responses to radiation doses, identifying key features such as voxel Skewness that correlate with tumor control and patient outcomes, suggesting its potential as a universal marker for assessing cross-cancer radiation effects.

Remarkably, despite internally controlled, standardized image acquisition protocols, many features extracted were unstable to temporal and spatial perturbations, emphasizing the importance of rigorous stability testing even when evaluating intra-patient changes with standardized imaging acquisition parameters. Notably, features like Skewness and LargeDependenceHighGrayLevelEmphasis consistently altered across treatment, showing these variations might indicate cumulative radiation effects. Radiomic features that are sensitive to dose change, like Skewness, could have utility in response prediction due to their quantifiable change. Additionally, associations between skewness and LFFS in this study and prior work [13] suggest its potential as a cross-cancer predictive marker for therapy efficacy. The conditional inference tree divided the patients into high and low risk groups by an optimal threshold of skewness ratio = 0.973 (Fig. 3), which was similar to the prior reported threshold for predicting failure in pancreatic cancer (0.951) [13]. We hypothesize that voxel Skewness may reflect intra-tumoral heterogeneity, with its variation during treatment indicating local response effectiveness. Further work is ongoing to investigate how intensity histogram feature Skewness and other textural features specifically correlate with cellular heterogeneity. For multivariate survival models, radiomics features were more highly concordant with local failure outcomes than overall progression or survival, suggesting these changes reflect local phenomena. Given the early stage of data collection and aggregation for MR-guided delta radiomics, and the small, heterogeneous patient population in this study, further validation will be necessary to confirm these findings, are hypothesis-generating. We expect our findings and methodologies will underpin broader radiomic validation studies in larger cohorts across malignancy types.

Our work advances the nascent field of RT delta radiomics, building on preliminary research and expanding beyond previous CT-based studies with limited outcomes [22,23]. Before our study, only one study explored MR-guided RT delta radiomics in pancreatic SBRT, [13], demonstrating predictive potential of features like Skewness. We expand the investigation of MR delta radiomics to lung cancer and are the first to systematically evaluate radiomic feature trajectories after both temporal and spatial stability testing.

This study has several limitations. Its small, single-institution sample size may introduce selection bias, and its confinement to one single MRI sequence, which, while promoting reproducibility, may limit generalizability. Our analysis focuses on linear relationships between inter-fraction radiomic values and their association with radiation delivery, while between RT-induced cellular change and radiographic manifestation may be more complex and non-linear. Additionally, our dataset was too small to compare total dose differences (between 40 and 60 Gy). Additionally, interpreting radiomic associations with outcomes beyond local control requires caution due to our cohort's large proportion of Stage IV patients. Despite heterogeneous radiomic feature responses through treatment, further work will be needed to validate specific delta radiomic patterns and signatures that consistently (and reproducibly) track with RT-induced cellular change. Future research should also investigate additional techniques, such as advanced machine learning methods and the use of image filters before feature extraction to increase the number of features that may highlight more detailed and comprehensive image properties [24,25]. Since we found skewness can potentially track dose response, nonspatial filters like taking the square or exponential could be used to adjust the sensitivity of skewness-related radiomics features to intensity values [25]. Deep learning may provide an attractive means for outcome prediction by delta radiomic features

Table 3
Multivariate Survival Analysis Result.

Survival	Delta radiomic feature (F5/F1)	p-value	HR (95 % CI)	Importance	Concordance
PFS					0.68
	Elongation	**0.04**	1.21 (1.01–1.45)	1	
	Flatness	0.15	0.86 (−0.71 to 1.05)	2	
	90Percentile	0.06	0.97 (0.93–1.00)	4	
	lmc2	**0.01**	1.20 (1.04–1.39)	3	
OS					0.63
	Elongation	0.43	1.09 (0.88–1.37)	2	
	Flatness	0.63	0.94 (0.75–1.19)	3	
	SurfaceVolumeRatio	0.81	0.98 (0.81–1.18)	4	
	DependenceEntropy	0.16	1.20 (0.93–1.57)	1	
LFFS					0.9
	Elongation	**0.02**	1.70 (1.10–2.65)	2	
	Flatness	0.18	0.74 (0.48–1.15)	3	
	DependenceEntropy	0.82	1.08 (0.56–2.06)	4	
	RunLengthNonUniformityNormalized	0.32	1.67 (0.61–4.57)	1	
ILFFS					0.85
	Elongation	0.07	1.25 (0.99–1.59)	2	
	Median	0.91	1.00 (0.93–1.09)	3	
	Imc2	0.08	1.53 (0.95–2.46)	1	
	DependenceEntropy	0.38	0.65 (0.24–1.71)	4	

[26], though necessitates larger datasets than presently available for effective model training.

In conclusion, our study demonstrates a feasible and stable delta radiomics pipeline for MR-guided lung SBRT that can serve as a framework for future cancer radiomics investigations. We find that MR-delta radiomic features change heterogeneously with distinct trajectories across tumors and that several may be indicative of RT-related tumoral change with increasing dose delivered, as well as risk of recurrence. Further work should validate these findings to determine if delta radiomics can ultimately serve as real-time, clinical biomarkers to guide personalized radiation regimens and therapeutic strategies.

Author contributions

Study design: Y.Z., B.H.K.; code design, implementation and execution: Y.Z., B.H.K.; acquisition, analysis or interpretation of data: Y.Z., B.H.K., Z.Y., A.Z., J.H., S.H.H.; statistical analysis: Y.Z., B.H.K.; writing of the manuscript: Y.Z., B.H.K.; critical revision of the manuscript for important intellectual content: all authors; study supervision: B.H.K.

Data availability

Although raw MR imaging data cannot be shared, all measured results to replicate the statistical analysis will be shared once the manuscript is accepted for publication.

Code availability

The codes of the delta-radiomics pipeline and statistical analysis are available at: https://github.com/AIM-KannLab/lung_cancer_radiomics.

Declaration of competing interest

The authors declare the following financial interests/personal relationships which may be considered as potential competing interests: Benjamin Kann, Raymond Mak, Shu-Hui Hsu, and Jonathan Leeman receive research support from ViewRay, Inc, not directly related to the work reported in this paper.

Appendix A. Supplementary data

Supplementary data to this article can be found online at https://doi.org/10.1016/j.phro.2024.100626.

References

[1] Siegel RL, Miller KD, Wagle NS, Jemal A. Cancer statistics, 2023. CA Cancer J Clin 2023;73:17–48. https://doi.org/10.3322/caac.21763.

[2] Timmerman R, Paulus R, Galvin J, Michalski J, Straube W, Bradley J, et al. Stereotactic body radiation therapy for inoperable early stage lung cancer. JAMA 2010;303:1070–6. https://doi.org/10.1001/jama.2010.261.

[3] Palma DA, Nguyen TK, Louie AV, Malthaner R, Fortin D, Rodrigues GB, et al. Measuring the integration of stereotactic ablative radiotherapy plus surgery for early-stage non-small cell lung cancer: A phase 2 clinical trial. JAMA Oncol 2019;5:681–8. https://doi.org/10.1001/jamaoncol.2018.6993.

[4] Weykamp F, Hoegen P, Regnery S, Katsigiannopulos E, Renkamp CK, Lang K, et al. Long-term clinical results of MR-guided stereotactic body radiotherapy of liver metastases. Cancers 2023;15. https://doi.org/10.3390/cancers15102786.

[5] Chen H, Han Z, Luo Q, Wang Y, Li Q, Zhou L, et al. Radiotherapy modulates tumor cell fate decisions: a review. Radiat Oncol 2022;17:196. https://doi.org/10.1186/s13014-022-02171-7.

[6] Sun MRM, Brook A, Powell MF, Kaliannan K, Wagner AA, Kaplan ID, et al. Effect of stereotactic body radiotherapy on the growth kinetics and enhancement pattern of primary renal tumors. AJR Am J Roentgenol 2016;206:544–53. https://doi.org/10.2214/AJR.14.14099.

[7] Yan M, Wang W. A radiomics model of predicting tumor volume change of patients with stage III non-small cell lung cancer after radiotherapy. Sci Prog 2021;104. https://doi.org/10.1177/0036850421997295.

[8] Gillies RJ, Kinahan PE, Hricak H. Radiomics: images are more than pictures, they are data. Radiology 2016;278:563–77. https://doi.org/10.1148/radiol.2015151169.

[9] Liu Z, Zhang X-Y, Shi Y-J, Wang L, Zhu H-T, Tang Z, et al. Radiomics analysis for evaluation of pathological complete response to neoadjuvant chemoradiotherapy in locally advanced rectal cancer. Clin Cancer Res Off J Am Assoc Cancer Res 2017;23:7253–62. https://doi.org/10.1158/1078-0432.CCR-17-1038.

[10] Cusumano D, Boldrini L, Yadav P, Casà C, Lee SL, Romano A, et al. Delta radiomics analysis for local control prediction in pancreatic cancer patients treated using magnetic resonance guided radiotherapy. Diagnostics 2021;11. https://doi.org/10.3390/diagnostics11010072.

[11] van Timmeren JE, van Elmpt W, Leijenaar RTH, Reymen B, Monshouwer R, Bussink J, et al. Longitudinal radiomics of cone-beam CT images from non-small cell lung cancer patients: Evaluation of the added prognostic value for overall survival and locoregional recurrence. Radiother Oncol 2019;136:78–85. https://doi.org/10.1016/j.radonc.2019.03.032.

[12] Lee G, Han Z, Huynh E, Tjong MC, Cagney DN, Huynh MA, et al. Widening the therapeutic window for central and ultra-central thoracic oligometastatic disease with stereotactic MR-guided adaptive radiation therapy (SMART). Radiother Oncol 2024;190:110034. https://doi.org/10.1016/j.radonc.2023.110034.

[13] Tomaszewski MR, Latifi K, Boyer E, Palm RF, El Naqa I, Moros EG, et al. Delta radiomics analysis of Magnetic Resonance guided radiotherapy imaging data can enable treatment response prediction in pancreatic cancer. Radiat Oncol 2021;16:237. https://doi.org/10.1186/s13014-021-01957-5.

[14] Collins GS, Reitsma JB, Altman DG, Moons KG. Transparent reporting of a multivariable prediction model for individual prognosis or diagnosis (TRIPOD): the TRIPOD Statement. BMC Med 2015;13:1. https://doi.org/10.1186/s12916-014-0241-z.

[15] van Griethuysen JJM, Fedorov A, Parmar C, Hosny A, Aucoin N, Narayan V, et al. Computational radiomics system to decode the radiographic phenotype. Cancer Res 2017;77:e104–7. https://doi.org/10.1158/0008-5472.CAN-17-0339.

[16] Zwanenburg A, Vallières M, Abdalah MA, Aerts HJWL, Andrearczyk V, Apte A, et al. The image biomarker standardization initiative: standardized quantitative radiomics for high-throughput image-based phenotyping. Radiology 2020;295:328–38. https://doi.org/10.1148/radiol.2020191145.

[17] Tustison NJ, Avants BB, Cook PA, Zheng Y, Egan A, Yushkevich PA, et al. N4ITK: improved N3 bias correction. IEEE Trans Med Imaging 2010;29:1310–20. https://doi.org/10.1109/TMI.2010.2046908.

[18] Benjamini Y, Hochberg Y. Controlling the false discovery rate: A practical and powerful approach to multiple testing. J R Stat Soc Ser B Methodol 1995;57:289–300. https://doi.org/10.1111/j.2517-6161.1995.tb02031.x.

[19] Guyon I, Weston J, Barnhill S, Vapnik V. Gene selection for cancer classification using support vector machines. Mach Learn 2002;46:389–422. https://doi.org/10.1023/A:1012487302797.

[20] Harrell FEJ, Lee KL, Mark DB. Multivariable prognostic models: issues in developing models, evaluating assumptions and adequacy, and measuring and reducing errors. Stat Med 1996;15:361–87. https://doi.org/10.1002/(SICI)1097-0258(19960229)15:4<361::AID-SIM168>3.0.CO;2-4.

[21] Adjogatse D, Petkar I, Reis Ferreira M, Kong A, Lei M, Thomas C, et al. The impact of interactive MRI-based radiologist review on radiotherapy target volume delineation in head and neck cancer. AJNR Am J Neuroradiol 2023;44:192–8. https://doi.org/10.3174/ajnr.A7773.

[22] Li Q, Kim J, Balagurunathan Y, Liu Y, Latifi K, Stringfield O, et al. Imaging features from pretreatment CT scans are associated with clinical outcomes in nonsmall-cell lung cancer patients treated with stereotactic body radiotherapy. Med Phys 2017;44:4341–9. https://doi.org/10.1002/mp.12309.

[23] Li Q, Kim J, Balagurunathan Y, Qi J, Liu Y, Latifi K, et al. CT imaging features associated with recurrence in non-small cell lung cancer patients after stereotactic body radiotherapy. Radiat Oncol Lond Engl 2017;12:158. https://doi.org/10.1186/s13014-017-0892-y.

[24] Demircioğlu A. The effect of preprocessing filters on predictive performance in radiomics. Eur Radiol Exp 2022;6:40. https://doi.org/10.1186/s41747-022-00294-w.

[25] Shur JD, Doran SJ, Kumar S, Ap Dafydd D, Downey K, O'Connor JPB, et al. Radiomics in oncology: A practical guide. Radiogr Rev Publ Radiol Soc N Am Inc 2021;41:1717–32. https://doi.org/10.1148/rg.2021210037.

[26] Dudas D, Saghand PG, Dilling TJ, Perez BA, Rosenberg SA, El Naqa I. Deep learning-guided dosimetry for mitigating local failure of patients with non-small cell lung cancer receiving stereotactic body radiation therapy. Int J Radiat Oncol Biol Phys 2023. https://doi.org/10.1016/j.ijrobp.2023.11.059. S0360-3016(23)08185-3.